Atomic Fermi Gas in the Trimerized Kagomé Lattice at 2/3 Filling

B. Damski,[1,2] H.-U. Everts,[1] A. Honecker,[3] H. Fehrmann,[1] L. Santos,[4] and M. Lewenstein[1,5,*]

[1]*Institut für Theoretische Physik, Universität Hannover, Appelstrasse 2, D-30167 Hannover, Germany*
[2]*Instytut Fizyki, Uniwersytet Jagielloński, Reymonta 4, PL-30-059 Kraków, Poland*
[3]*Institut für Theoretische Physik, TU Braunschweig, Mendelssohnstrasse 3, D-38106 Braunschweig, Germany*
[4]*Institut für Theoretische Physik III, Universität Stuttgart, Pfaffenwaldring 57 V, D-70550 Stuttgart, Germany*
[5]*ICFO-Institut de Ciències Fotòniques, Jordi Girona 29, Edifici Nexus II, E-08034 Barcelona, Spain*

(Received 6 December 2004; published 5 August 2005)

We study low temperature properties of a spinless interacting Fermi gas in the trimerized kagomé lattice. The case of two fermions per trimer is described by a quantum spin 1/2 model on the triangular lattice with couplings depending on the bond directions. Using exact diagonalizations we show that the system exhibits nonstandard properties of a *quantum spin-liquid crystal*, combining a planar antiferromagnetic order with an exceptionally large number of low-energy excitations.

DOI: 10.1103/PhysRevLett.95.060403 PACS numbers: 05.30.Fk, 03.75.Ss

One of the most fascinating recent trends in physics of ultracold gases concerns atomic gases in optical lattices, where strongly correlated systems may be realized. Such systems offer an ''atomic Hubbard toolbox'' [1] to simulate various sorts of Hubbard models, and to study phenomena known in condensed matter physics in an unprecedently controlled manner. To name just a few examples, atomic lattice gases may serve to study various spin models [2], to simulate high T_c superconductivity [3], to investigate a variety of quantum disordered systems [4], or to process quantum information [5]. Seminal experiments of Ref. [6] have stimulated a great interest in experimental studies of atomic lattice gases (cf. [7]).

Particularly fascinating in this context is the possibility of studying quantum frustrated antiferromagnets, which lie at the heart of modern quantum magnetism [8]. Recently we have proposed how to create ideal and trimerized kagomé optical lattices, and have studied physics of various quantum gases in such lattices [9]. A Fermi-Fermi mixture with half filling for both species in the limit of strong interspecies coupling behaves in the ideal kagomé lattice as a spin 1/2 Heisenberg antiferromagnet (KAF). Such a system (having so far no experimental realization among solid state systems) is a paradigmatic, although not yet fully understood (cf. [10]) example of a quantum spin liquid of type II [11].

In Ref. [9] we have also discussed briefly the case of an interacting spinless Fermi gas in the trimerized kagomé lattice at filling 2/3 (2 atoms per trimer). Such a system behaves as a quantum magnet on the triangular lattice with couplings that depend on bond directions, and is particularly interesting since: (i) it describes the physics of the trimerized KAF in the plateau region at one-third of the saturation magnetization [12]; (ii) it has itself fascinating properties, expected to be generic for ''multimerized'' frustrated systems; (iii) it is a paradigmatic Fermi system to study in trimerized lattices; (iv) it is experimentally feasible. In this Letter we study the low temperature physics of this system using exact diagonalizations of the Hamiltonian for $12, \ldots, 24$ spins. We show that for effectively ferromagnetic couplings the system exhibits the nonstandard properties of a *quantum spin-liquid crystal,* combining planar antiferromagnetic order with an exceptionally large number of low-energy excitations, and a small (if any) gap. For the effectively antiferromagnetic coupling the *quantum* results agree very well with the *classical* results indicating antiferromagnetic planar order and a gapped spectrum.

The experimental realization of the considered system requires a creation of trimerized kagomé lattice, using superlattice techniques as shown in Ref. [9]. The spinless interacting Fermi gas can then be formed, for instance, in a Bose-Fermi mixture, in the strong coupling limit, when bosons form a Mott insulator (MI), and fermions together with $0, 1, \ldots$ bosons (bosonic holes) form fermionic composites [13]. Alternatively, one could use a gas of polarized ultracold dipolar fermions that interact via a repulsive dipolar potential.

The spinless interacting Fermi gas in the trimerized kagomé lattice is described by the extended Fermi-Hubbard Hamiltonian $H_{\mathrm{FH}} = -\Sigma_{\langle ab\rangle}(t_{ab} f_a^\dagger f_b + \mathrm{H.c.}) + \Sigma_{\langle ab\rangle} U_{ab} n_a n_b$, where $a = \{\alpha, i\}$ with α referring to intratrimer indices and i numbering the trimers. The t_{ab} and U_{ab} take the values t and U for intratrimer, and t' and U' for intertrimer hopping, $n_a = f_a^\dagger f_a$, and f_a is the fermionic annihilation operator. The sites in each trimer are enumerated as in Fig. 1(a). We denote the three different intratrimer modes by $f^{(i)} = (f_{1,i} + f_{2,i} + f_{3,i})/\sqrt{3}$ (zero momentum mode), and $f_\pm^{(i)} = (f_{1,i} + z_\pm f_{2,i} + z_\pm^2 f_{3,i})/\sqrt{3}$ (left and right chirality modes), where $z_\pm = \exp(\pm 2\pi i/3)$.

In the limit of weak coupling between the trimers of the original kagomé lattice, the problem of two fermions per trimer (filling 2/3) becomes equivalent to a quantum magnet on a triangular lattice with couplings that depend on the bond directions as described by the Hamiltonian

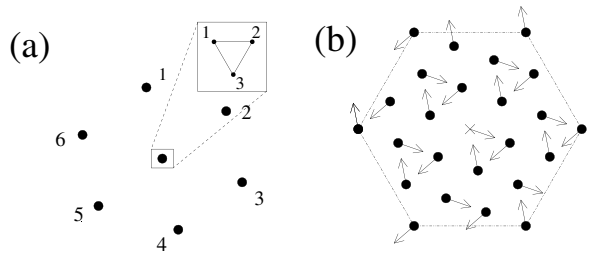

FIG. 1. (a) Enumeration of intertrimer (intratrimer) nearest neighbors. (b) Classical 120° state with *left* chirality.

$$H_{\text{trimer}} = \frac{J}{2}\sum_{i=1}^{N}\sum_{j=1}^{6} s_i(\phi_{i\to j}) s_j(\tilde{\phi}_{j\to i}), \qquad (1)$$

where N denotes number of trimers, $J = 4U'/9$, and the nearest neighbors are enumerated as in Fig. 1(a). In Eq. (1) we have $s_i(\phi) = \cos(\phi)s_x^{(i)} + \sin(\phi)s_y^{(i)}$, where the spin-1/2 operators $s_x^{(i)}$, $s_y^{(i)}$ are defined as $s_x^{(i)} = (f_+^{(i)\dagger} f_-^{(i)} + f_-^{(i)\dagger} f_+^{(i)})/2$, $s_y^{(i)} = -i(f_+^{(i)\dagger} f_-^{(i)} - f_-^{(i)\dagger} f_+^{(i)})/2$. The angles ϕ are $\phi_{i\to 1} = \phi_{i\to 6} = 0$, $\phi_{i\to 2} = \phi_{i\to 3} = 2\pi/3$, $\phi_{i\to 4} = \phi_{i\to 5} = -2\pi/3$, $\tilde{\phi}_{1\to i} = \tilde{\phi}_{2\to i} = -2\pi/3$, $\tilde{\phi}_{3\to i} = \tilde{\phi}_{4\to i} = 0$, $\tilde{\phi}_{5\to i} = \tilde{\phi}_{6\to i} = 2\pi/3$. This Hamiltonian has previously appeared in the context of a block-spin approach to the Heisenberg KAF [14,15]. The main purpose of that approach has been to find the origin of the exponentially large number of low-lying singlets that had been found in numerical studies of the kagomé antiferromagnet [16,17]. From Refs. [14,15] it also follows that H_{trimer} describes the physics of the trimerized KAF in a magnetic field that drives this system into the plateau region at 1/3 of the saturation magnetization. We stress that the Hamiltonian H_{trimer} to be studied in this Letter describes *a physically feasible situation.*

Let us begin by discussing the classical theory of the model (1), which describes the large spin limit. In addition to being translationally invariant, the model of Eq. (1) is invariant under the point group of order 6, $Z_6 = Z_3 Z_2$, where the generator of Z_3 (order 3) is the combined rotation of the lattice by the angle $4\pi/3$, and of the spins by the angle $2\pi/3$, while the generator of Z_2 (order 2) is the spin inversion in the x-y plane. We note that our model possesses no continuous spin rotational symmetry. There exist three ordered classical states with small unit cells that are compatible with this point-group symmetry of the model: a ferromagnetic state, and two 120° Néel type structures with left [Fig. 1(b)] and right [Fig. 2(a)] chiralities. The energies per site of these states are $E_{\text{class}}^{\text{ferro}} = E_{\text{class}}^{\text{right}} = -3S^2J/4$ and $E_{\text{class}}^{\text{left}} = 3S^2J/2$, where the subscripts "right" and "left" refer to chiralities. Hence, for $J < 0$ the state with left-handed chirality will be the ground state (GS). For $J > 0$ the situation is more complex: the states with right-handed chirality and the ferromagnetic state are degenerate ground states.

To understand further the classical ground states we analyzed numerically the 12-spin cell by fixing the direction of every spin to $n\pi/3$ ($n = 0, \ldots, 5$), and checking the energies of the resulting 6^{12} configurations. This analysis has revealed that for $J < 0$ there are 6 ground states [Z_6 symmetry of (1)], each of them exhibiting the left chirality Néel order. For $J > 0$ the results are dramatically different: there are 240 degenerate classical GSs in this case, among them 6 pure right chirality Néel states and 6 purely ferromagnetic states. For an illustration we show in Fig. 3 two ordered GSs with very large unit cells [Figs. 3(b) and 3(d)] together with their parent states [Figs. 3(a) and 3(c)]. The large number of degenerate *classical* GSs finds its analogue in a large density of low-lying excitations of the *quantum* version of Eq. (1).

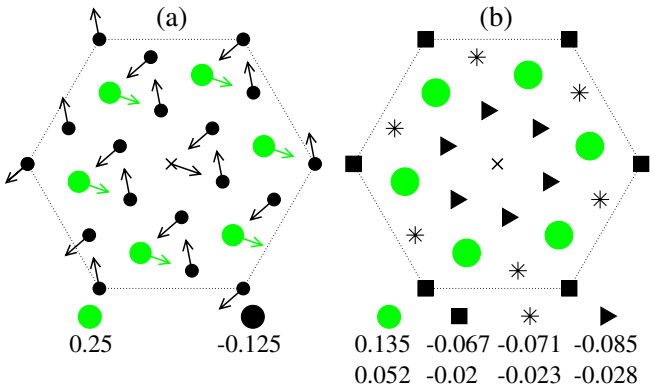

FIG. 2 (color online). (a) Classical 120° state with *right* chirality. Dots show $s_x^{(i)}s_x^{(10)} + s_y^{(i)}s_y^{(10)}$, where $|\vec{s}| = 1/2$ [22]; (b) spin-spin correlations, $\langle s_x^{(i)}s_x^{(10)} + s_y^{(i)}s_y^{(10)}\rangle$. The upper (lower) set of values corresponds to $kT = 0$ ($kT = 10^{-2}J/2$). In both plots $N = 21$ and $i = 10$ at the central site.

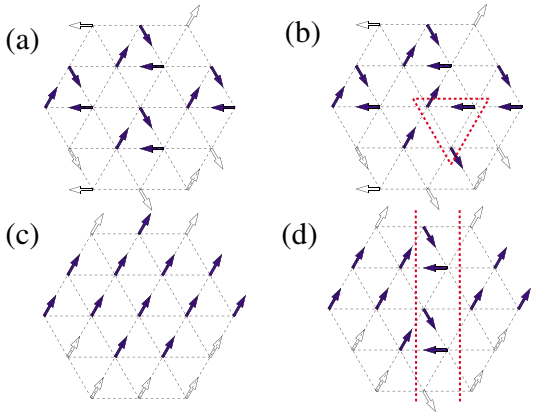

FIG. 3 (color online). (a) Right chirality Néel configuration; (b) localized defect in configuration (a); (c) ferromagnetic configuration; (d) line defect in configuration (c). Open arrows present spins determined by the boundary conditions for the 12-spin cell. Defects are marked by red dashed contours.

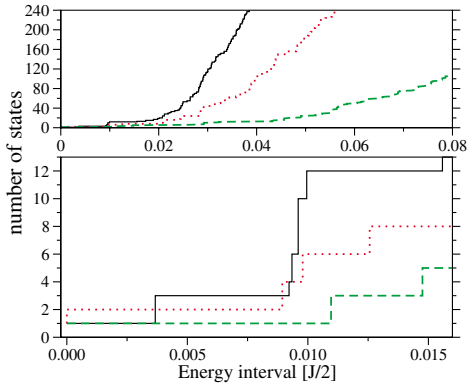

FIG. 4 (color online). Number of states in an energy interval above the GS: black (solid), red (dotted), and green (dashed) lines for $N = 24, 21$, and 18, respectively.

To describe the physics of spinless fermions on a trimerized optical kagomé lattice at filling $2/3$ we need to consider the model, Eq. (1), for spin $1/2$, i.e., in the extreme quantum limit. Questions to be answered for this case are the following: (i) Is the GS of the model Eq. (1) an ordered state, or is it a spin liquid either of type I, i.e., a state without broken symmetry, with exponentially fast decaying spin-pair correlations and a gap to the first excitation, or of type II, i.e., a kagomé-like GS again without broken symmetry, with extremely short ranged correlations, but with a dense spectrum of excitations adjacent to the GS. (ii) What are the thermal properties of our system? After all, the model can be realized only at finite, albeit low temperatures.

To answer the above questions we have performed exact diagonalization of the Hamiltonian (1) for $N = 12, 15, 18, 21$, and 24 spins using the ARPACK routines [18]. To simplify the calculations, we block diagonalized the Hamiltonian (1) by exploiting its translational symmetries, thereby reducing the dimensions of the matrices that had to be diagonalized from $2^N \times 2^N$ to $\approx 2^N/N \times 2^N/N$. Despite all these efforts, studies of larger systems require the use of massive computer resources. Fortunately, the results for 21 and 24 spins show qualitative and quantitative resemblance, and we regard them as representative for larger systems.

Our findings are presented in Figs. 2(b) and 4 and Tables I and II. For $J > 0$, in contrast to the classical result, the ground state exhibits the 120° Néel order with right chirality [19]. This is illustrated in Fig. 2(b), where the planar spin-spin correlations are presented. Direct comparison with the correlations of the classical state, Fig. 2(a), shows that the exact quantum correlations, although smaller, have the same order of magnitude and sign as the classical ones. Especially, the relative values of correlations compare nicely to the classical result: Table I summarizes the results for $N = 21$ and $N = 24$. Amazingly, the 120° Néel order survives at finite temperatures, as is indicated by the results obtained for $kT = 10^{-2}J/2$; see Fig. 2(b). At such temperatures about 800 low-energy eigenstates contribute to the correlations. For smaller systems, $N < 21$ ($J > 0$), finite size effects affect the spin correlations strongly. Nevertheless, the ground state energy per spin can be reliably extracted from the data for $N \geq 12$, resulting in $-0.2175J - 0.0755J/N$.

The selection of a GS with 120° planar Néel order from the large manifold of classical GSs by quantum effects implies the breaking of the translational and of the point group of our model Eq. (1), but there is no continuous symmetry that the ordered GS could break. Therefore, the standard expectation would be that the excitations have a gap of the order of J. Instead, we find that the system has an exceptionally large number of low-energy excitations (see Fig. 4). For instance, for $N = 21$ in the energy interval $0.1J/2$ there are about 800 excited states. Most of them support the spin order of the GS so that this order persists at finite temperatures.

The analysis of the results for different N's are compatible with an exponential increase of the number of low-energy states with the system size N similarly as in the case of the $S = 1/2$ KAF [16,17]. For the KAF Mila has been able to explain this high density of low-energy states by associating them approximately with dimer coverings of an effective triangular lattice with uncorrelated products of nearest-neighbor pair states [15]. His method fails here, because the low-lying states of our model must certainly be highly correlated. On account of the breaking of the discrete symmetries of our model by the Néel order, one expects the ground state of the *infinite* system to be sixfold degenerate. For *finite* systems this degeneracy is lifted. Nevertheless, we expect to find six low-lying states in the gap below the lowest excited state. In view of this scenario, the inspection of the lower panel of Fig. 4 suggests that the gap, if any, is smaller than $10^{-2}J/2$. The appearance of this very small energy scale is completely unexpected and puzzling. Obviously, the answer to the questions (i) and (ii) above is that the GS is ordered and that the order

TABLE I. Planar spin-spin correlations for $J > 0$ as a function of distance $1, \ldots, 3$ in lattice units.

	1	$\sqrt{3}$	2	$\sqrt{7}$	3
120°	−0.125	0.25	−0.125	−0.125	0.25
$N = 24$	−0.096	0.162	−0.083	−0.080	0.156
$N = 21$	−0.085	0.135	−0.071	−0.067	

TABLE II. Planar spin-spin correlations for $J < 0$ as a function of distance $1, \ldots, \sqrt{7}$ in lattice units.

	1	$\sqrt{3}$	2	$\sqrt{7}$
120°	−0.125	0.25	−0.125	−0.125
$N = 21$	−0.134	0.237	−0.117	−0.116
$N = 12$	−0.137	0.251	−0.125	

survives at low T. The smallness of the gap and the large density of low-energy states, however, resemble very much the behavior of a quantum spin liquid of type II. For these reasons we propose to term our system a *quantum spin-liquid crystal.* We note, in this context, that the specific heat of the $N = 21$ system exhibits a peak at $kT \sim 7 \times 10^{-3} J/2$.

The above results for $J > 0$ contrast dramatically with those for $J < 0$, summarized in Table II. In the latter case we deal with the standard quantum antiferromagnet with 120° Néel order and left chirality [19] [Fig. 1(b)]. The spectrum is gapped, and the classical spin-spin correlations approximate the quantum correlations remarkably well. The gap is of the order $|J|/2$ in this case ($N = 12, 18, 21$), meaning that there are at most a few states with energies substantially below $|J|/2$ for $J < 0$, as opposed to the huge number for $J > 0$ (Fig. 4).

The observation of physics described in this Letter requires achieving low, but not unrealistic $T \simeq 10$ to 100 nK (cf. Ref. [13]). In experiments N could vary from $\simeq 20$ to $\simeq 1000$. The low-energy states may be prepared by employing adiabatic changes of the degree of trimerization of the lattice. For instance, one can start with a completely trimerized lattice; the filling $\nu = 2/3$ may be achieved then by starting with $\nu = 1$, and eliminating 1 atom per trimer using, for instance, laser excitations. One can then increase t and U slowly, on the time scale smaller than the final $1/J$ ($\simeq$ seconds). Alternatively, one could start with $\nu \simeq 2/3$ in the moderately trimerized regime. As in Ref. [6], the inhomogeneity of the lattice due to the trapping potential, would then allow one to achieve the Mott state with $\nu = 2/3$ per trimer in the center of the trap. Nearly perfect $2/3$ filling can be achieved by loading a Bose-Einstein condensate of molecules formed by 2 fermions into a triangular lattice, generating an MI state, adiabatically transforming the lattice to a trimerized kagomé one, ''dissociating'' the molecules by changing the scattering length to negative values, and by finally optically pumping the atoms into a single internal state. Preparing $\nu = 2/3$ might involve undesired heating (due to optical pumping), which can be overcome by using laser, or phonon cooling afterwards (cf. [20]). Note that the imperfections of ν can be described by a ''t-J'' kind of model, and are of interest themselves.

After preparation it should then be possible to measure the energy of the system simply by opening the lattice; by repeated measurement of the energy $E(T)$ at (definite) finite temperatures one would get in this way an access to the density of modes, i.e., could compare the results with Fig. 4. From such measurements one could infer about the existence of the gap E_{gap}, since if E_{gap} is large enough, $E(T)$ becomes T independent for $kT \leq E_{\mathrm{gap}}$. Various other correlations could be measured as proposed in Ref. [21]. In order to measure planar spin correlations, one has, however, to lift the degeneracy of the $f_{\pm}$ modes, e.g., by slightly modifying the intensity of one of the superlattices forming the trimerized lattice. This should be done on a time scale faster than the characteristic time scales of other interactions, so that the state of the system would not change during the measurement. In such a case one can use far off resonant Raman scattering (or scattering of matter waves) to measure the dynamic structure factor, proportional to the spatiotemporal Fourier transform of the density-density correlations. At frequencies close to the Raman resonance between the $f_{\pm}$ modes, only $f_{+} - f_{-}$ transitions contribute to the signal, and hence such measurement yields the desired information about the correlations $\langle f_{+}^{(i)\dagger} f_{-}^{(i)} f_{-}^{(j)\dagger} f_{+}^{(j)} \rangle$ and the spin correlations of Fig. 2.

A. H. is indebted to D. C. Cabra and P. Pujol for collaboration related to the present work. We acknowledge support from the Deutsche Forschungsgemeinschaft (SFB 407, SPP1116, 436 POL), ESF Programme QUDEDIS, and the Alexander von Humboldt Foundation.

*Also at Institució Catalana de Recerca i Estudis Avançats.

[1] D. Jaksch *et al.*, Phys. Rev. Lett. **81**, 3108 (1998); D. Jaksch and P. Zoller, Ann. Phys. (N.Y.) **315**, 52 (2005).
[2] L.-M. Duan, E. Demler, and M. D. Lukin, Phys. Rev. Lett. **91**, 090402 (2003).
[3] W. Hofstetter *et al.*, Phys. Rev. Lett. **89**, 220407 (2002).
[4] B. Damski *et al.*, Phys. Rev. Lett. **90**, 110401 (2003); A. Sanpera *et al.*, *ibid.* **93**, 040401 (2004).
[5] J. I. Cirac and P. Zoller, Phys. Today **57**, No. 3, 38 (2004).
[6] M. Greiner *et al.*, Nature (London) **415**, 39 (2002).
[7] S. Peil *et al.*, Phys. Rev. A **67**, 051603(R) (2003); J. V. Porto *et al.*, Phil. Trans. R. Soc. A **361**, 1417 (2003).
[8] G. Misguich and C. Lhuillier, in *Frustrated Spin Systems*, edited by H. T. Diep (World Scientific, Singapore, 2005).
[9] L. Santos *et al.*, Phys. Rev. Lett. **93**, 030601 (2004).
[10] P. Nikolic and T. Senthil, Phys. Rev. B **68**, 214415 (2003).
[11] P. Sindzingre, C. Lhuillier, and J.- B. Fouet, Int. J. Mod. Phys. B **17**, 5031 (2003).
[12] D. C. Cabra *et al.*, Phys. Rev. B **71**, 144420 (2005).
[13] H. Fehrmann *et al.*, Opt. Commun. **243**, 23 (2004).
[14] V. Subrahmanyam, Phys. Rev. B **52**, 1133 (1995).
[15] F. Mila, Phys. Rev. Lett. **81**, 2356 (1998); M. Mambrini and F. Mila, Eur. Phys. J. B **17**, 651 (2000).
[16] P. Lecheminant *et al.*, Phys. Rev. B **56**, 2521 (1997).
[17] Ch. Waldtmann *et al.*, Eur. Phys. J. B **2**, 501 (1998).
[18] http://www.caam.rice.edu/software/ARPACK/.
[19] The chirality is found from $\langle s_x^{(i)} s_y^{(j)} - s_y^{(i)} s_x^{(j)} + s_x^{(j)} s_y^{(k)} - s_y^{(j)} s_x^{(k)} + s_x^{(k)} s_y^{(i)} - s_y^{(k)} s_x^{(i)} \rangle$, where i, j, k enumerate sites of the smallest triangular substructures; see S. Miyashita, Prog. Theor. Phys. Suppl. **87**, 112 (1986).
[20] A. J. Daley, P. O. Fedichev, and P. Zoller, Phys. Rev. A **69**, 022306 (2004).
[21] J. J. García-Ripoll, M. A. Martin-Delgado, and J. I. Cirac, Phys. Rev. Lett. **93**, 250405 (2004).
[22] The central spin in Fig. 2(a) defines the x axis.